Climate of the Past

Open Access

Discussions

Persistent decadal-scale rainfall variability in the tropical South Pacific Convergence Zone through the past six centuries

C. R. Maupin[1,2], J. W. Partin[1], C.-C. Shen[3], T. M. Quinn[1,2], K. Lin[3], F. W. Taylor[1], J. L. Banner[2], K. Thirumalai[1,2], and D. J. Sinclair[4]

[1]Institute for Geophysics, Jackson School of Geosciences, University of Texas, Austin, Texas 78758, USA
[2]Department of Geological Sciences, Jackson School of Geosciences, University of Texas, Austin, Texas 78705, USA
[3]High-Precision Mass Spectrometry and Environment Change Laboratory (HISPEC), Department of Geosciences, National Taiwan University, Taipei 106, ROC, Taiwan
[4]Institute of Marine and Coastal Sciences, Rutgers University, New Brunswick, New Jersey 08901, USA

Correspondence to: C. R. Maupin (crmaupinatx@neo.tamu.edu)

Discussion Paper | Discussion Paper | Discussion Paper | Discussion Paper |

CPD

9, 5593–5625, 2013

Persistent decadal-scale rainfall variability

C. R. Maupin et al.

Title Page

Abstract | Introduction

Conclusions | References

Tables | Figures

◀◀ | ▶▶

◀ | ▶

Back | Close

Full Screen / Esc

Printer-friendly Version

Interactive Discussion

Abstract

Observations and reconstructions of decadal-scale climate variability are necessary to place predictions of future global climate change into temporal context (Goddard et al., 2012). This is especially true for decadal-scale climate variability that originates in the
5 Pacific Ocean (Deser et al., 2004; Dong and Lu, 2013). We focus here on the western tropical Pacific (Solomon Islands; $\sim 9.5°$ S, $\sim 160°$ E), a region directly influenced by: the South Pacific Convergence Zone (SPCZ), the West Pacific Warm Pool (WPWP), the Pacific Walker Circulation (PWC), and the Hadley Circulation. We calibrate δ^{18}O variations in a fast growing stalagmite to local rainfall amount and produce a 600 yr
10 record of rainfall variability from the zonally oriented, tropical portion of the SPCZ. We present evidence for large (~ 1.5 m), persistent and decade(s)-long shifts in total annual rainfall amount in the Solomon Islands since 1416 ± 5 CE. The timing of the decadal changes in rainfall inferred from the 20th century portion of the stalagmite δ^{18}O record coincide with previously identified decadal shifts in Pacific ocean-atmosphere behavior
15 (Clement et al., 2011; Deser et al., 2004). The 600 yr Solomons stalagmite δ^{18}O record indicates that decadal oscillations in rainfall are a robust characteristic of SPCZ-related climate variability, which has important implications to water resource management in this region.

1 Introduction

20 ### 1.1 Significance of an SPCZ paleoclimate reconstruction

Decadal-scale climate variability in the Pacific is intimately linked with global climate variability, and is a critical factor in infrastructure and resource management planning (Cane, 2010; Dong and Lu, 2013; Goddard et al., 2012). The South Pacific Convergence Zone (SPCZ) is the primary source of rainfall to Pacific island communities as
25 well as one of the largest sources of heat and moisture to the atmosphere (Dong

and Lu, 2013; Kiladis et al., 1989; Matthews, 2011; Vincent, 1994). Climate regime shifts are rapid transitions in decadal climate state between distinct epochs (Deser et al., 2004). These shifts, such as the well-studied occurrence in 1976/1977, manifest as changes in a suite of climate system phenomena, including movement, rainfall and cloudiness in the SPCZ, Pacific Walker Circulation (PWC) strength, tropical and subtropical sea surface temperature (SST) anomalies termed the Interdecadal Pacific Oscillation, or IPO, (Folland et al., 2002), and shallow Pacific meridional overturning circulation (Cane, 2010; Dong and Lu, 2013; Folland et al., 2002; Goddard et al., 2012; Matthews, 2011; Vincent, 1994; Widlansky et al., 2010).

Multiple mechanisms have been proposed to explain the source of the decadal-to multidecadal-scale variability in the Pacific. However, a consensus has not been reached on the mechanism responsible. One hypothesis states that changes in the number of sunspots, which occur in distinct ∼ 11 yr cycles, may elicit, or at least correspond to, significant rainfall changes in the equatorial SPCZ region (Meehl et al., 2009). Timing of peak sunspot numbers during the last three 11 yr solar cycles have been associated with periods of strengthened rainfall in the SPCZ region (Meehl et al., 2009). Other hypotheses include (1) feedbacks from reduced trade-wind strength and low-level convergence in the central and eastern tropical Pacific (Clement et al., 2011), (2) the integration of stochastic forcing or El Niño-Southern Oscillation (ENSO) asymmetry by the ocean mixed layer (Clement et al., 2011), and (3) decadal-scale subtropical to tropical exchange of water masses or strength of the shallow overturning that drives this exchange (Gu and Philander, 1997; McPhaden and Zhang, 2004; Zhang and McPhaden, 2006).

The SPCZ is a recognized carrier of the atmospheric signal of decadal-scale variability over the instrumental period. Rainfall and cloudiness changes in the SPCZ region are relatively large and coherent with basin- and decadal-scale ocean and atmosphere variability (Clement et al., 2011; Deser et al., 2004; Dong and Lu, 2013). Atmospheric and precipitation variability on timescales from many decades to centuries in the tropical region of the SPCZ remains poorly constrained despite this important

SPCZ characteristic. Indeed, only three distinct decadal phases are identifiable in instrumental data (Deser et al., 2004), and only the latter half of the twentieth century contains significant spatial coverage of meteorological data for the tropical Pacific (L'Heureux et al., 2013). The SPCZ has, as a result, been identified as a critical target location for paleoclimate reconstructions of atmospheric behavior on interannual and decadal timescales (Deser et al., 2004). Such reconstructions are crucial for establishing whether the large amplitude oscillations in rainfall amount are persistent, and whether they remain stationary through time.

1.2 Modern climate setting in the Solomon Islands

The Solomon Islands are positioned within the confluence of SPCZ rainfall (Folland et al., 2002; Vincent, 1994; Widlansky et al., 2010), the rising limb of the PWC and Hadley circulations (Matthews, 2011; Takahashi and Battisti, 2007), and the WPWP SST (Rayner et al., 2003). The Solomons have mean annual SSTs greater than 28 °C, often used as a criteria for the boundary of the WPWP (Cravatte et al., 2009; Rayner et al., 2003).

Rainfall variability in the broader tropical SPCZ region is well represented by rainfall variability at the study site. Connection of regional variability with local rainfall requires using a short (1998–2011), high resolution ($0.25° \times 0.25°$) satellite-measured rainfall amount from the Tropical Rainfall Measuring Mission TRMM (Kummerow et al., 2000). Monthly anomalies are significantly correlated with anomalies in the broader tropical SPCZ domain (Fig. 1b, c). Rainfall amount over the study site does exhibit seasonality, with sixty-five percent of mean total annual rainfall (TAR, 2.10 ± 0.41 m, 1σ, 1952–1989) occurring during December through April. These local rainfall observations are based on a monthly rain gauge record from Henderson Airfield, which is located 10 km northeast of Forestry Cave, on Guadalcanal. We note that even in May through November, rainfall is still appreciable.

The primary mechanisms by which rainfall amounts change in the Solomon Islands are twofold: (1) displacement of the SPCZ southwestward or northeastward and (2)

changes in the amount of rainfall within the SPCZ independent of its position (Clement et al., 2011; Deser et al., 2004; Folland et al., 2002). The period from 1977 through 1995 vs. 1947 through 1976 had reduced rainfall amounts (0.5 mTAR reduction in the Henderson Airfield rain gauge) and cloudiness within, as well as a northeastward and equatorward movement of the SPCZ after the 1976/1977 shift. Both displacement and reduced intensity of the SPCZ result in reduced rainfall amount at the study site. Deconvoluting the effects of movement- and convection-related changes in rainfall amount in the tropical SPCZ requires climate records from multiple locations in the poleward and equatorward flanks of the Solomon Islands (Deser et al., 2004). The coherent response over the Solomon Islands to the rainfall changes triggered by decadal variability make it a well-suited location to begin to reconstruct the decadal signal carried by the tropical portion of the SPCZ.

1.3 Stalagmite time series from Guadalcanal, Solomon Islands

Here we present a U-series dated, $\delta^{18}O$ record of rainfall variability from 2010 to 1416 ± 5 CE in fast-growing cave calcite deposits (stalagmites) from the northern coast of Guadalcanal, Solomon Islands. We demonstrate that stalagmite $\delta^{18}O$ variations can be interpreted as variations in rainfall amount through the tropical "amount effect", an empirical relationship whereby greater rainfall amounts lead to more depleted rainfall $\delta^{18}O$, and thus the $\delta^{18}O$ of calcite precipitated from this water (Dansgaard, 1964; Gat, 1996; Partin et al., 2012; Rozanski et al., 1993). We quantitatively calibrate this amount effect in our stalagmite record via the local rainfall record and use it to place the nearly 600 yr long $\delta^{18}O$ record into meteorological context in order to assess the character of rainfall variability through the past six centuries. This record provides new perspective on tropical SPCZ rainfall variability applicable to resource management and infrastructure preparation for the Solomon Islands, where fresh water availability is restricted to the volume of a surface lens that is dependent on rainfall amount. It also provides constraints for decadal range climate model projections.

2 Methods

2.1 Sample collection and description

Two stalagmites, 10FC-02 and 05FC-04, were collected from Forestry Cave, northwestern Guadalcanal (9°29′19.50″ S, 159°58′25.56″ E). The cave is located ∼ 200 m a.s.l. on the northern slope of Mount Austen, 2.5 km south of Barana Village. The slope vegetation consists of dense tropical forest. The cave entrance is positioned on the southwest side of a ∼ 20 m deep streamed ravine that runs from southeast to northwest. The back of the cave has an elevated (∼ 2 m above the cave floor), highly decorated ledge 25–30 m from the entrance. A rimstone dam forms the face of the ledge. The 10FC-02 sample was collected in August 2010 from this plateau and was in growth position, with an active drip. The 05FC-04 sample used for replication testing (see Sect. 2.4) is a small "candlestick" stalagmite that was collected broken from the floor of the plateau in November 2005. X-ray diffraction (XRD) analysis performed on several powdered subsamples of the 10FC-02 stalagmite show prominent calcite peaks and no aragonite peaks.

Dripwaters were collected from both Forestry Cave (9°29′19.50″ S, 159°58′25.56″ E) and nearby Jacob's Cave (9°29′12.42″ S, 159°58′23.88″ E) during the same two-week period of August 2010, when the 10FC-02 sample was collected. Although none of the Forestry Cave drips came from directly above the 10FC-02 sample, they were collected within 3 m of the sample site. Forestry Cave and Jacob's Cave are ∼ 200 m apart on the northern slope of Mount Austen and are in the same ravine at the same elevation.

2.2 Isotopic analyses

Samples for stable isotopic analysis were continuously milled from the stalagmite at 500 µm increments (Fig. 2). This yielded 2140 samples, excluding samples within overlaps used to align different paths. Average temporal resolution of the each sample is ∼ 4 months (seasonal resolution) of calcite precipitation based on the average growth rate.

Aliquots of each sample, 25–80 µg, were analyzed for δ^{18}O and δ^{13}C using a Thermo Electron Kiel IV automated carbonate device connected to a Thermo Electron MAT253 dual inlet isotope ratio mass spectrometer (IRMS) housed in the Analytical Laboratory for Paleoclimate Studies (ALPS) at the Jackson School of Geosciences, University of

5 Texas at Austin. Stable isotopic ratios of carbonate samples are reported in per mil units vs. VPDB. The long-term average precision for these analyses is ±0.12 (2σ) for δ^{18}O and ±0.06 (2σ) for δ^{13}C. Dripwater δ^{18}O analyses were performed using a Gasbench II attached to a Conflo IV and a Thermo Electron Delta V Plus IRMS, also housed in ALPS. All isotopic ratios for water samples are reported in per mil vs. VSMOW. Preci-

10 sion for these water analyses is ±0.20 (2σ) for δ^{18}O.

U-Th dates were determined from stalagmite samples (0.150–1.008 g) on a Thermo Electron Neptune multi-collector inductively coupled plasma mass spectrometer (MC-ICP-MS) housed in the High-Precision Mass Spectrometry and Environment Change (HISPEC) Laboratory at the National Taiwan University (Shen et al., 2012). Analyses

15 of the 10FC-02 stalagmite samples have an average analytical error of 8.8 yr (±2σ).

2.3 Age model

The growth history of the 10FC-02 stalagmite is constrained by a total of 41 U-Th dates. A Monte Carlo method of constructing alternate age models ($N = 10\,000$) by fitting cubic splines to the U-Th dates and their ±2σ age uncertainty provides an ap-

20 proach amenable to the difficulty of U-Th dating such young material (Fig. 3). The number of knots ($N = 8$), which are places where the piecewise polynomials connect, for the spline fitting was selected to minimize the error in the numerical fit while preventing stratigraphic inversions from arising in the median reconstructed growth history. Increasing the number of knots increases the fit of the median age model to the U-

25 Th dates and reduces mean uncertainty in the growth history reconstruction, but can come at the cost of introducing age inversions in the age model. This method allows construction of an age model that accounts for apparent age inversions of spatially

Title Page

Abstract   Introduction

Conclusions   References

Tables   Figures

|◄   ►|

◄   ►

Back   Close

Full Screen / Esc

Printer-friendly Version

Interactive Discussion

close U-Th dates in a fast growing, relatively young stalagmite with low U-content. It further provides a method of estimating temporal uncertainty for each individual δ^{18}O point in the time series.

We use a replication method of verifying the robustness of the climate signal in addition to the "Hendy Test" (Hendy, 1971). Individual paths in the 10FC-02 are not in the same place with respect to the centerline of the stalagmite slabs, and comparing δ^{18}O where paths overlap with one another provides a Hendy Test. There is no δ^{18}O offset between paths that lie toward the margins of the stalagmite vs. the center of the stalagmite (Fig. 2), indicating that where sampled, the 10FC-02 is free of intra-sample non-climatic effects, such as non-equilibrium fractionation and mixed mineralogy. We perform a replication test by generation of century-long time series of δ^{18}O and δ^{13}C variations from the 05FC-04 stalagmite. We use four U-Th dates and the Monte Carlo method described above, with four knots, to reconstruct the 05FC-04 growth history. We then align salient features in the δ^{18}O record of the 05FC-04 to the 10FC-02 δ^{18}O time series without exceeding the 2σ age uncertainties of the U-Th dates. We use this approach as it has been shown to be robust relative to the traditional single-growth layer Hendy Test (Dorale and Liu, 2009), for which concerns are raised regarding the feasibility of accurately sampling a single growth layer. Vegetation and other controls can influence dripwater δ^{13}C in addition to the unlikelihood that two stalagmites have undergone identical kinetic processes. There are also doubts regarding whether invariable δ^{18}O profiles across a single growth layer are robust evidence for an absence of kinetic fractionation. All of these points are cited as justifications for using replication to test stalagmite δ^{18}O climate signal fidelity (Dorale and Liu, 2009; Feng et al., 2012).

2.4 Assessing non-climatic controls on stalagmite δ^{18}O variability

We investigate multiple lines of evidence to assess whether the stalagmite δ^{18}O variations record environmental conditions above the cave, which ultimately means the stalagmite reflects changes in rainfall δ^{18}O. First, we assess whether the calcite δ^{18}O formed in isotopic equilibrium with the cave dripwater δ^{18}O by calculating the expected

equilibrium calcite δ^{18}O values using dripwater δ^{18}O values and a mean annual temperature for Honiara of 26.5 °C±0.1 °C (as calculated from 1952–1989 meteorological station data from Honiara, GISTEMP, http://data.giss.nasa.gov/gistemp/station_data/). We use both inorganic, laboratory-based (Kim and O'Neil, 1997) and empirical, cave-based water-calcite (Tremaine et al., 2011) fractionation equations to perform these calculations, summarized in Table S2. We acknowledge that the laboratory equation predicts calcite δ^{18}O values that are depleted relative to the observed calcite δ^{18}O. Depletion in cave calcite δ^{18}O relative to laboratory equilibrium is well documented (Feng et al., 2012; Tremaine et al., 2011) and has been attributed to differences between typical stalagmite deposition temperatures in cave environments and the temperature ranges of laboratory experiments, as well as stalagmite growth rate (Feng et al., 2012; Mickler et al., 2006). The δ^{18}O value predicted from the Tremaine et al. (2011) cave-based fractionation equation falls within error of the δ^{18}O$_{\text{calcite}}$ measured at the tip of 10FC-02. The tip δ^{18}O sample includes the top 500 µm of the 10FC-02 stalagmite and may represent an average value for at least the preceding ∼ 3 months.

Next we assess whether or not calcite δ^{18}O, which reflects cave dripwater δ^{18}O, is in fact recording rainfall δ^{18}O changes above the cave. The δ^{18}O signal in the second Forestry Cave stalagmite (05FC-04) is a close match in terms of mean and variability to the δ^{18}O record in the first stalagmite: a demonstration of the reproducibility of the climate signal (Fig. 4a). Stalagmite δ^{13}C variations show none of the decadal variability exhibited by the δ^{18}O record and the two records are only weakly correlated (R^2 = 0.11, Fig. 4a, b). The controls on stalagmite δ^{13}C are more complicated, and the contrast of the disagreement between the two stalagmites δ^{13}C records and the agreement between the two δ^{18}O records further increases our certainty that stalagmite δ^{18}O is recording a common signal: rainfall δ^{18}O. We conclude from the above analyses that the stalagmite δ^{18}O best reflects rainfall δ^{18}O composition over the stalagmite growth interval.

Full Screen / Esc

Printer-friendly Version

Interactive Discussion

2.5 Source effect on rainfall $\delta^{18}O$

We investigate whether moisture source effects might complicate the relationship between rainfall amount and rainfall $\delta^{18}O$ by examining the potential pathways and sources of water vapor to the Solomons. We use model results from mid-month of the peak-dry season (August and September) and mid-month of the peak-wet season (February and March) from 2007–2009 (HYSPLIT, http://www.arl.noaa.gov/HYSPLIT.php). The resulting trajectories show possible air parcel paths and potential vapor sources ranging from the equatorial Pacific to the southeastern tropical and southern subtropical Pacific. These trajectories represent a broad range of potential water vapor sources, transit distances, mean and seasonal SST regimes, all over an interval of time where stalagmite $\delta^{18}O$ changes by only 0.3 ‰. This suggests that variability in source is not an important factor in controlling rainfall $\delta^{18}O$ in the modern setting.

3 Results and implications

3.1 Calibration of stalagmite $\delta^{18}O$ to rainfall amount

We use the Henderson Airfield rain gauge on Guadalcanal, as well as a rain gauge record from Auki, on the nearby island of Malaita, 112 km northeast of Forestry Cave (Fig. 5a) to calibrate stalagmite $\delta^{18}O$ with local rain gauge observations. It would be ideal to have contemporaneous rainfall amount, rainfall $\delta^{18}O$, cave dripwater $\delta^{18}O$ and stalagmite $\delta^{18}O$ time series. However, as we do not have time series of rainfall $\delta^{18}O$ or dripwater $\delta^{18}O$, we establish in Sect. 2.4 that stalagmite $\delta^{18}O$ records changes in rainfall $\delta^{18}O$. Therefore, we use this relationship to calibrate the changes in stalagmite $\delta^{18}O$ (i.e., rainfall $\delta^{18}O$) to rainfall amount. We calculate the dependence of stalagmite $\delta^{18}O$ changes on changes in total annual rainfall amount through robust maximum likelihood linear regression (Thirumalai et al., 2011) of means and corresponding

standard errors from both rain gauge records against contemporaneous means and standard errors in the stalagmite δ^{18}O record. This regression calibrates the two variables ($r = -0.92$, $n = 5$) with a slope of $1.4 \pm 0.3\,‰\,\text{mTAR}^{-1}$ (Fig. 5). Annual rainfall totals were calculated, as opposed to means or anomalies, for purposes of comparison to the stalagmite record. Annual totals were only calculated for years where gauge observations exist for all 12 months of the year. This result is consistent with the relationship between rainfall amount and rainfall δ^{18}O of $1.2\,‰\,\text{mTAR}^{-1}$ observed at the closest available Global Network of Isotopes in Precipitation GNIP, (IAEA, 2006) site in Madang, Papua New Guinea, 1650 km to the west northwest of Guadalcanal. Rainfall δ^{18}O and rainfall amount from Guam have been documented to have a broadly similar relationship of $1.18 \pm 0.31\,‰\,\text{mTAR}^{-1}$ (Partin et al., 2012).

3.2 Characterizing the rainfall reconstruction

Our stalagmite δ^{18}O/rainfall amount calibration (Fig. 5) reveals that rainfall variability in the Solomons is characterized by large, abrupt, periodic increases and decreases in precipitation amount on decadal to multidecadal timescales over the past six centuries. The transitions from these periods of high to low rainfall amounts evolve abruptly (< 20 yr) every 12 to 62 yr. Rectified wavelet (Fig. 6), Monte Carlo-singular spectrum analysis (MC-SSA), and multi-taper method (MTM) analyses (Liu et al., 2007; Torrence and Compo, 1998) all independently confirm the oscillatory nature of the proxy rainfall record. The MTM (Fig. 7) and wavelet analyses reveal persistent concentrations of power at decadal periodicities, significant ($p < 0.05$ for the wavelet and $p < 0.01$ in the MTM) above an AR(1) red noise model. The SSA, performed with a window length of 100 and broken into 50 components, shows that 84 % of the variance in the record is decadal in nature (12 to 62 yr). The wavelet spectrum also shows significant power in the annual to interannual band, when stalagmite growth is rapid enough, demonstrating that karst processes are not reddening shorter timescale variability to longer timescales to cause the decadal variability in the stalagmite δ^{18}O record. The spectral analyses emphasizes that decadal variability is distinct, and is not red noise

Title Page

Abstract | Introduction

Conclusions | References

Tables | Figures

|◀ | ▶|

◀ | ▶

Back | Close

Full Screen / Esc

Printer-friendly Version

Interactive Discussion

arising from integration of higher frequency stochastic processes or ENSO modulation to longer timescales (Clement et al., 2011; Deser et al., 2004; Miller and Schneider, 2000; Newman et al., 2003). We acknowledge that the significant periodicity could be an artifact from the sampling of a limited time window. Such significance may not persist
5 in a longer times series, and thus the system behavior would be characterized as a red noise process. Given the 600 yr record length, and the many occurrences of decadal- to multidecadal-scale variability therein, however, we conclude that the stalagmite is recording variability that likely arises from non-stochastic processes.

   The well-studied transition in 1976/1977 of Pacific climate represents a relatively
10 small change when compared to many of such shifts observed throughout the Solomons rainfall reconstruction. For example, the 1976/1977 transition of ~ 0.6 ‰ in the stalagmite δ^{18}O record corresponds to a reduction of 0.5 mTAR, or a 22 % relative decrease in rainfall. The stalagmite δ^{18}O record contains other decadal transitions in the pre-instrumental era that routinely reach or exceed 1.5 mTAR, or ~ 2.4 ‰. This is
15 approximately three times larger than the wet-to-dry transition in 1976/1977. This is re- flected by rainfall extrema that exceed the intervals on either side of the 1976/1977 tran- sition. The interval from 1977–1998 in the rain gauge record indicates a multidecadal dry interval with an average of 1.7 mTAR. Such drier periods in the pre-instrumental era tend to exhibit rainfall totals of ~ 1.4 mTAR. The pre-1977 wet period in the rain gauge
20 time series averages 2.2 mTAR, however precipitation in pre-instrumental stalagmite- reconstructed wet phases reached amounts as high as 2.8 mTAR.

   The nineteenth and twentieth centuries in the stalagmite δ^{18}O record, which overlaps with portions of the instrumental record, exhibits a shift to longer period multidecadal- scale variability. The most recent portion of the wavelet is within the "cone of influence"
25 (Dong and Lu, 2013; Kiladis et al., 1989; Matthews, 2011; Torrence and Compo, 1998; Vincent, 1994), so caution is advisable when interpreting the lower frequency vari- ability in comparison to the preceding centuries that is readily observed in the time do- main, particularly from ~ 1890 to 1950 CE. We suggest that this may represent a recent

change in system behavior with possible origins in very long (multicentury-scale) modulation in decadal- and multidecadal-scale variability (Deser et al., 2004).

3.3 External forcing vs. internal variability

We also test the hypothesis that variations in sunspot number acts to elicit a rainfall response in the SPCZ region (Cane, 2010; Dong and Lu, 2013; Folland et al., 2002; Goddard et al., 2012; Matthews, 2011; Meehl et al., 2009; Vincent, 1994; Widlansky et al., 2010), by examining the relationship between stalagmite δ^{18}O variations at our study site and variations in sunspot number. Spectral analysis of the stalagmite δ^{18}O record reveals significant concentration of power at 11 yr. We use a Gaussian window to bandpass-filter the stalagmite time series at 11 yr (0.0909 ± 0.02 (bandwidth) cycles yr^{-1}) and compare it to available sunspot counts since 1749 (Fig. 8). The comparison shows no consistent relationship in amplitude or phasing of the two records. Indeed, over the course of the 262 yr of comparison, one can identify decades when the two records are in phase, out of phase and when they have various lead/lag relations. Hence we conclude that rainfall variability at the study site is not a result of forcing related to the 11 yr solar cycle. We note that the interpretations of (Meehl et al., 2009) are based on comparisons between rainfall variability in the SPCZ over the three most recent sunspot cycles; an interval over which the filtered stalagmite δ^{18}O and sunspot records are in phase. However, this in–phase relationship breaks down between $\sim$ 1800 and 1930 as well as during other times (Fig. 8c).

We conclude that the decadal to multidecadal-scale oscillations observed in the stalagmite reconstruction most likely arise as a consequence of internal variability in the ocean-atmosphere climate system of the Pacific and are not forced by solar changes. Such internal variability drives large changes in rainfall amount over the study site as a consequence of changes in SPCZ strength and SPCZ movement. There is no consistent response by rainfall amount to the decadal-scale, periodic external forcing of sunspot counts. This interpretation is consistent with the majority of the hypotheses that reach a conclusion of an internal causative mechanism internal to the

ocean-atmosphere system that drives the observed decadal-scale regime shifts over the instrumental record in the Pacific (Clement et al., 2011; Gu and Philander, 1997; Meehl et al., 2009; Zhang and McPhaden, 2006).

3.4 Phase changes in the instrumental record and the stalagmite record

The timing of recent decadal shifts in SPCZ rainfall documented by the Solomon Islands stalagmite record is broadly consistent with the timing of phase changes (wet phases: ??–1924, 1947–1976; and dry phases: 1925–1946, 1977–1995) in other relevant tropical Pacific instrumental time series: the IPO index of SST, equatorial central Pacific SST, as well as the zonal Pacific SLP gradient, where robust SLP data are available (∼ 1950 to present; Clement et al., 2011; L'Heureux et al., 2013). This SLP gradient in the tropical Pacific has been taken as a surface expression of the PWC (Clement et al., 2011; Dong and Lu, 2013; Vecchi and Soden, 2007; Vecchi et al., 2006). The beginning of the 1925/26 regime shift appears to occur earlier in the stalagmite δ^{18}O record. The reason for this could be due limitations in instrumental data density and quality in the Pacific. Stalagmite age model uncertainties are fairly small for this time interval (±1.2 yr in 1925). Schematically, a weakening in the thermally direct Walker circulation means less latent heat flux into the atmosphere by trade-wind-driven evaporative cooling (Allen and Ingram, 2002; Clement et al., 2011; Gu and Philander, 1997; McPhaden and Zhang, 2004; Vecchi and Soden, 2007; Zhang and McPhaden, 2006). This reduced tradewind strength would likely allow a northeastward displacement of the SPCZ. Additionally, the reduced latent heat flux into the atmosphere means that less rainfall in the tropical SPCZ and WPWP deep convection regions satisfies the radiation budget.

Coral-based reconstructions of sea surface salinity and SST also document robust decadal-scale variability (Clement et al., 2011; Deser et al., 2004; Dong and Lu, 2013; Gorman et al., 2012; Kilbourne et al., 2004; Linsley et al., 2006, 2008; Wu et al., 2013).The surface ocean changes recorded by corals, however, are not a direct reconstruction of rainfall, nor necessarily the atmospheric phenomena that drive rainfall

Title Page

Abstract | Introduction

Conclusions | References

Tables | Figures

◄ | ►

◄ | ►

Back | Close

Full Screen / Esc

Printer-friendly Version

Interactive Discussion

variability The level of stationarity of relative contributions to study site rainfall changes via (1) movement of the SPCZ vs. (2) rainfall amount within the SPCZ remains a point for clarification. Addressing this uncertainty requires further spatial coverage of climate reconstructions, necessitating additional paleoclimate records of rainfall variabil-
5   ity. Hence, the two different proxy approaches to reconstruct SPCZ variability in the pre-instrumental period are complementary.

4   Summary and conclusions

Rainfall is predicted to increase by 9–20 % for the tropical SPCZ region in the next century due to anthropogenic influences (Deser et al., 2004; Perkins et al., 2012). It is
10   therefore important to note that even a 20 % rainfall increase in the future is less than a third of the relative changes in rainfall amount that has occurred naturally on decadal timescales over the past six centuries based on our proxy-based rainfall reconstruction. The large decadal changes in rainfall over the Solomon Islands appear linked with other phase changes identified in the instrumental records for a range of Pacific ocean and
15   atmosphere phenomena in the Pacific Basin. The variability in the rainfall reconstruction is important for testing climate model skill as well as informing future projections. Furthermore, future occurrences of such large, decades-long changes in rainfall within the SPCZ and WPWP, deserve careful consideration when arriving at strategies for infrastructure development and resource management in the SPCZ region as well as the
20   many regions that are teleconnected to Pacific decadal variability (Deser et al., 2004; Garreaud and Battisti, 1999; L'Heureux et al., 2013; Zhang et al., 1997).

In this study, we have presented a new, U-series dated, instrumentally calibrated, stalagmite-based proxy record of rainfall amount in the Solomon Islands. The Solomons stalagmite δ^{18}O reconstruction of rainfall clearly establishes that large
25   amplitude oscillations in rainfall amount are persistent, and that they remain stationary at decadal to multidecadal timescales over the last 600 yr. These oscillatory phase changes show no relationship to the periodic external forcing of sunspot

cycles, suggesting a stationary mechanism of internal forcing. Changes identified in the relatively short instrumental window of tropical Pacific climate are present in the most recent portion of the stalagmite record. The best studied of these changes, the 1976/1977 regime shift, has rainfall changes in the Solomons that are one third the amplitude (0.5 mTAR) of past phase changes (1.5 mTAR) during the last 600 yr. The relatively large amplitude changes in rainfall should be considered in resource management planning, climate model validation, and predictions of anthropogenically forced changes in the Pacific hydroclimate.

Predicted values were calculated using dripwater δ^{18}O values, experimental, laboratory-based as well as cave-based, empirical dripwater-calcite fractionation equations (Kim and O'Neil, 1997; Kummerow et al., 2000; Tremaine et al., 2011) and mean annual temperature for Honiara from 1952–1989 (26.5 °C ± 0.1 °C, 1se) from GISTEMP station data. Forestry Cave and Jacob's Cave are ∼ 200 m apart on the northern slope of Mount Austen and are in an identical setting. The tip δ^{18}O value is the measured value for the top 500 µm of the 10FC-02 stalagmite and represents an average value for the preceding ∼ 3 months. Predicted and measured values of δ^{18}O calcite fall within even error of each other using the cave-based equation even when only accounting for analytical uncertainty.

References

Allen, M. R. and Ingram, W. J.: Constraints on future changes in climate and the hydrologic cycle, Nature, 419, 224–232, doi:10.1038/nature01092, 2002.

Cane, M. A.: Climate science: decadal predictions in demand, Nat. Geosci., 3, 231–232, doi:10.1038/ngeo823, 2010.

Cheng, H., Edwards, R. L., Hoff, J., Gallup, C. D., Richards, D. A., and Asmerom, Y.: The half-lives of uranium-234 and thorium-230, Chem. Geol., 169, 17–33, 2000.

Clement, A., DiNezio, P., and Deser, C.: Rethinking the Ocean's Role in the Southern Oscillation, J. Climate, 24, 4056–4072, doi:10.1175/2011JCLI3973.1, 2011.

Cravatte, S., Delcroix, T., Zhang, D., Mcphaden, M., and Leloup, J.: Observed freshening and warming of the western Pacific Warm Pool, Clim. Dynam., 33, 565–589, doi:10.1007/s00382-009-0526-7, 2009.

Dansgaard, W.: Stable isotopes in precipitation, Tellus, 16, 436–468, 1964.

Deser, C., Phillips, A., and Hurrell, J.: Pacific interdecadal climate variability: Linkages between the tropics and the North Pacific during boreal winter since 1900, J. Climate, 17, 3109–3124, 2004.

Dong, B. and Lu, R.: Interdecadal enhancement of the walker circulation over the Tropical Pacific in the late 1990s, Adv. Atmos. Sci., 30, 247–262, doi:10.1007/s00376-012-2069-9, 2013.

Dorale, J. A. and Liu, Z.: Limitations of Hendy test criteria in judging the paleoclimatic suitability of speleothems and the need for replication, J. Cave Karst Stud., 71, 73–80, 2009.

Feng, W., Banner, J. L., Guilfoyle, A. L., Musgrove, M., and James, E. W.: Oxygen isotopic fractionation between drip water and speleothem calcite: a 10 yr monitoring study, Central Texas, USA, Chem. Geol., 304–305, 53–67, doi:10.1016/j.chemgeo.2012.02.004, 2012.

Folland, C., Renwick, J., Salinger, M., and Mullan, A.: Relative influences of the Interdecadal Pacific Oscillation and ENSO on the South Pacific Convergence Zone, Geophys. Res. Lett., 29, 1643, doi:10.1029/2001GL014201, 2002.

Garreaud, R. D. and Battisti, D. S.: Interannual (ENSO) and interdecadal (ENSO-like) variability in the Southern Hemisphere tropospheric circulation, J. Climate, 12, 2113–2123, 1999.

Gat, J. R.: Oxygen and hydrogen isotopes in the hydrologic cycle, Annu. Rev. Earth. Planet. Sc., 24, 225–262, 1996.

Persistent decadal-scale rainfall variability

C. R. Maupin et al.

Title Page

Abstract | Introduction

Conclusions | References

Tables | Figures

|◄ | ►|

◄ | ►

Back | Close

Full Screen / Esc

Printer-friendly Version

Interactive Discussion

Goddard, L., Hurrell, J. W., Kirtman, B. P., Murphy, J., Stockdale, T., and Vera, C.: Two time scales for the price of one (almost), B. Am. Meteorol. Soc., 93, 621–629, doi:10.1175/BAMS-D-11-00220.1, 2012.

Gorman, M. K., Quinn, T. M., Taylor, F. W., Partin, J. W., Cabioch, G., Austin, J. A., Jr., Pelletier, B., Ballu, V., Maes, C., and Saustrup, S.: A coral-based reconstruction of sea surface salinity at Sabine Bank, Vanuatu from 1842 to 2007 CE, Paleoceanography, 27, PA3226, doi:10.1029/2012PA002302, 2012.

Gu, D. and Philander, S.: Interdecadal climate fluctuations that depend on exchanges between the tropics and extratropics, Science, 275, 805–807, 1997.

Hendy, C. H.: Isotopic geochemistry of speleothems: 1. calculation of effects of different modes of formation on isotopic composition of speleothems and their applicability as palaeoclimatic indicators, Geochim. Cosmochim. Ac., 35, 801–824, doi:10.1016/0016-7037(71)90127-X, 1971.

IAEA, G.: Global Network of Isotopes in Precipitation, the GNIP Database, available at: http://www.iaea.org/water (last access: 24 May 2012), 2006.

Jaffey, A. H., Flynn, K. F., Glendenin, L. E., Bentley, W. C., and Essling, A. M.: Precision measurement of half-lives and specific activities of U-235 and U-238, Phys. Rev. C, 4, 1889–1906, 1971.

Kiladis, G. N., von Storch, H., and van Loon, H.: Origin of the South-Pacific convergence zone, J. Climate, 2, 1185–1195, 1989.

Kilbourne, K., Quinn, T., Taylor, F., Delcroix, T., and Gouriou, Y.: El Nino-Southern oscillation-related salinity variations recorded in the skeletal geochemistry of a Porites coral from Espiritu Santo, Vanuatu, Paleoceanography, 19, PA4002, doi:10.1029/2004PA001033, 2004.

Kim, S.-T. and O'Neil, J. R.: Equilibrium and nonequilibrium oxygen isotope effects in synthetic carbonates, Geochim. Cosmochim. Ac., 61, 3461–3475, 1997.

Kummerow, C., Simpson, J., Thiele, O., Barnes, W., Chang, A., Stocker, E., Adler, R. F., Hou, A., Kakar, R., Wentz, F., Ashcroft, P., Kozu, T., Hong, Y., Okamoto, K., Iguchi, T., Kuroiwa, H., Im, E., Haddad, Z., Huffman, G., Ferrier, B., Olson, W. S., Zipser, E., Smith, E. A., Wilheit, T. T., North, G., Krishnamurti, T., and Nakamura, K.: The status of the Tropical Rainfall Measuring Mission (TRMM) after two years in orbit, J. Appl. Meteorol., 39, 1965–1982, 2000.

Linsley, B. K., Kaplan, A., Gouriou, Y., Salinger, J., Demenocal, P. B., Wellington, G. M., and Howe, S. S.: Tracking the extent of the South Pacific Convergence Zone since the early 1600s, Geochem. Geophy. Geosy., 7, Q05003, doi:10.1029/2005GC001115, 2006.

Persistent decadal-scale rainfall variability

C. R. Maupin et al.

Title Page

Abstract	Introduction
Conclusions	References
Tables	Figures

◀◀   ▶▶

◀   ▶

Back   Close

Full Screen / Esc

Printer-friendly Version

Interactive Discussion

Linsley, B. K., Zhang, P., Kaplan, A., Howe, S. S., and Wellington, G. M.: Interdecadal-decadal climate variability from multicoral oxygen isotope records in the South Pacific Convergence Zone region since 1650 AD, Paleoceanography, 23, PA2219, doi:10.1029/2007PA001539, 2008.

5 Liu, Y., Liang, X., and Weisberg, R. H.: Rectification of the bias in the wavelet power spectrum, J. Atmos. Oceanic Technol., 24, 2093–2102, doi:10.1175/2007JTECHO511.1, 2007.

L'Heureux, M. L., Lee, S., and Lyon, B.: Recent multidecadal strengthening of the Walker circulation across the Tropical Pacific, Nature Clim. Change, doi:10.1038/nclimate1840, 2013.

Matthews, A. J.: A multiscale framework for the origin and variability of the South Pacific Con-
10 vergence Zone, Q. J. Roy. Meteor. Soc., 1165–1178, doi:10.1002/qj.1870, 2011.

McPhaden, M. J. and Zhang, D.: Pacific Ocean circulation rebounds, Geophys. Res. Lett., 31, L18301, doi:10.1029/2004GL020727, 2004.

Meehl, G. A., Arblaster, J. M., Matthes, K., Sassi, F., and van Loon, H.: Amplifying the Pacific climate system response to a small 11 yr solar cycle forcing, Science, 325, 1114–1118,
15 doi:10.1126/science.1172872, 2009.

Mickler, P. J., Stern, L. A., and Banner, J. L.: Large kinetic isotope effects in modern speleothems, Geol. Soc. Am. Bull, 118, 65–81, doi:10.1130/B25698.1, 2006.

Miller, A. and Schneider, N.: Interdecadal climate regime dynamics in the North Pacific Ocean: theories, observations and ecosystem impacts, Prog. Oceanogr., 47, 355–379,
20 doi:10.1016/S0079-6611(00)00044-6, 2000.

Newman, M., Compo, G. P., and Alexander, M. A.: ENSO-forced variability of the Pacific decadal oscillation, J. Climate, 16, 3853–3857, 2003.

Partin, J. W., Jenson, J. W., Banner, J. L., Quinn, T. M., Taylor, F. W., Sinclair, D., Hardt, B., Lander, M. A., Bell, T., Miklaviè, B., Jocson, J. M. U., and Taboroši, D.: Relationship be-
25 tween modern rainfall variability, cave dripwater, and stalagmite geochemistry in Guam, USA, Geochem. Geophy. Geosy., 13, Q03013, doi:10.1029/2011GC003930, 2012.

Perkins, S., Irving, D., Brown, J., Power, S., Moise, A., Colman, R., and Smith, I.: CMIP3 ensemble climate projections over the western tropical Pacific based on model skill, Clim. Res., 51, 35–58, doi:10.3354/cr01046, 2012.

30 Rayner, N., Parker, D. E., Horton, E., Folland, C., Alexander, L., Rowell, D., Kent, E., and Kaplan, A.: Global analyses of sea surface temperature, sea ice, and night marine air temperature since the late nineteenth century, J. Geophys. Res.-Atmos., 108, 4407, doi:10.1029/2002JD002670, 2003.

Title Page

Abstract | Introduction

Conclusions | References

Tables | Figures

|◄ | ►|

◄ | ►

Back | Close

Full Screen / Esc

Printer-friendly Version

Interactive Discussion

Rozanski, K., Araguas-Araguas, L., and Gonfiantini, R.: Isotopic patterns in modern global precipitation, in: Climate Change in Continental Isotopic Records, American Geophysical Union, Washington, DC, 1–36, 1993.

Shen, C.-C., Wu, C.-C., Cheng, H., Edwards, R. L., Hsieh, Y.-T., Gallet, S., Chang, C.-C., Li, T.-Y., Lam, D. D., Kano, A., Hori, M., and Spötl, C.: High-precision and high-resolution carbonate ^{230}Th dating by MC-ICP-MS with SEM protocols, Geochim. Cosmochim. Ac., 99, 71–86, doi:10.1016/j.gca.2012.09.018, 2012.

Takahashi, K. and Battisti, D. S.: Processes controlling the mean tropical pacific precipitation pattern. Part II: The SPCZ and the southeast pacific dry zone, J. Climate, 20, 5696–5706, doi:10.1175/2007JCLI1656.1, 2007.

Thirumalai, K., Singh, A., and Ramesh, R.: A MATLAB Code to Perform Weighted Linear Regression with (correlated or uncorrelated) Errors in Bivariate Data, J. Geol. Soc. India, 77, 377–380, 2011.

Torrence, C. and Compo, G. P.: A practical guide to wavelet analysis, B. Am. Meteorol. Soc., 79, 61–78, 1998.

Tremaine, D. M., Froelich, P. N., and Wang, Y.: Speleothem calcite farmed in situ: Modern calibration of delta O-18 and delta C-13 paleoclimate proxies in a continuously-monitored natural cave system, Geochim. Cosmochim. Ac., 75, 4929–4950, doi:10.1016/j.gca.2011.06.005, 2011.

Vecchi, G. A. and Soden, B. J.: Global warming and the weakening of the tropical circulation, J. Climate, 20, 4316–4340, doi:10.1175/JCLI4258.1, 2007.

Vecchi, G., Soden, B., Wittenberg, A., Held, I., Leetmaa, A., and Harrison, M.: Weakening of tropical Pacific atmospheric circulation due to anthropogenic forcing, Nature, 441, 73–76, doi:10.1038/nature04744, 2006.

Vincent, D. G.: The South-Pacific Convergence Zone (SPCZ) – a review, Mon. Weather Rev., 122, 1949–1970, 1994.

Vose, R. S., Schmoyer, R. L., Steurer, P. M., Peterson, T. C., Heim, R., Karl, T. R., and Eischeid, J. K.: The Global Historical Climatology Network: long-term monthly temperature, precipitation, sea level pressure, and station pressure data, Oak Ridge National Laboratory, ORNL/CDIAC-53(NPD-041), doi:10.3334/CDIAC/cli.ndp041, 1992.

Widlansky, M. J., Webster, P. J., and Hoyos, C. D.: On the location and orientation of the South Pacific Convergence Zone, Clim. Dynam., 36, 561–578, doi:10.1007/s00382-010-0871-6, 2010.

Title Page

Abstract | Introduction

Conclusions | References

Tables | Figures

|◀ | ▶|

◀ | ▶

Back | Close

Full Screen / Esc

Printer-friendly Version

Interactive Discussion

Wu, H. C., Linsley, B. K., Dassié, E. P., Schiraldi Jr., B., and deMenocal, P. B.: Oceano-graphic variability in the South Pacific Convergence Zone region over the last 210 years from multi-site coral Sr/Ca records, Geochem. Geophys. Geosyst., 14, 1435–1453, doi:10.1029/2012GC004293, 2013.

5 Zhang, D. and McPhaden, M. J.: Decadal variability of the shallow Pacific meridional overturn-ing circulation: Relation to tropical sea surface temperatures in observations and climate change models, Ocean Model., 15, 250–273, doi:10.1016/j.ocemod.2005.12.005, 2006.

Zhang, Y., Wallace, J. M., and Battisti, D. S.: ENSO-like interdecadal variability: 1900–93, J. Climate, 10, 1004–1020, 1997.

Title Page

Abstract | Introduction

Conclusions | References

Tables | Figures

|◄ | ►|

◄ | ►

Back | Close

Full Screen / Esc

Printer-friendly Version

Interactive Discussion

Table 1. U-Th dates used to reconstruct 10FC-02 (top) and 05FC-04 (bottom) stalagmite growth histories.

10FC-02 Depth (cm)	Weight g	^{238}U ppb	^{232}Th ppt	δ^{234}U measured[a]	$[^{230}$Th/^{238}U] activity[c]	$[^{230}$Th/^{232}Th] ppm[d]	Age uncorrected	Year CE[c,e]	δ^{234}U$_{initial}$ corrected[b]
4.25	0.23210	204.56 ± 0.20	44.7 ± 3.0	6.7 ± 1.5	0.000432 ± 0.000044	32.7 ± 4.0	46.9 ± 4.8	1970.7 ± 5.6	6.7 ± 1.5
8.55	0.21507	295.76 ± 0.31	55.7 ± 3.2	9.8 ± 1.5	0.000679 ± 0.000035	59.5 ± 4.6	73.4 ± 3.8	1943.2 ± 4.6	9.8 ± 1.5
10.35	0.27735	333.41 ± 0.46	46.6 ± 2.5	6.0 ± 1.8	0.000528 ± 0.000032	62.3 ± 5.1	57.3 ± 3.5	1958.3 ± 4.0	6.0 ± 1.8
14.45	0.29840	213.00 ± 0.20	18.7 ± 2.3	5.5 ± 1.5	0.000738 ± 0.000056	138 ± 20	80.2 ± 6.1	1934.0 ± 6.2	5.5 ± 1.5
17.55	0.21002	204.01 ± 0.21	27.6 ± 3.3	6.6 ± 1.5	0.001004 ± 0.000049	123 ± 16	109.0 ± 5.3	1906.2 ± 5.6	6.6 ± 1.5
18.80	0.32690	289.38 ± 0.28	8.6 ± 2.1	7.0 ± 1.5	0.000984 ± 0.000038	544 ± 136	106.8 ± 4.1	1905.8 ± 4.1	7.0 ± 1.5
22.50	0.3247	193.43 ± 0.14	12.7 ± 2.1	6.8 ± 1.2	0.001164 ± 0.000042	293 ± 51	126.4 ± 4.6	1886.8 ± 4.7	6.8 ± 1.2
24.25	0.16750	359.22 ± 0.41	15.0 ± 4.2	5.1 ± 1.9	0.001127 ± 0.000046	447 ± 127	122.6 ± 7.0	1890.4 ± 7.0	5.1 ± 1.9
25.50	0.22171	281.05 ± 0.31	36.0 ± 3.1	6.3 ± 1.7	0.000992 ± 0.000046	128 ± 13	107.7 ± 5.0	1907.3 ± 5.3	6.3 ± 1.7
31.10	0.20897	217.47 ± 0.22	36.8 ± 3.3	5.0 ± 1.5	0.001422 ± 0.000052	139 ± 14	154.6 ± 5.7	1861.4 ± 6.1	5.0 ± 1.5
32.00	0.19800	212.61 ± 0.24	38.0 ± 3.5	9.5 ± 1.8	0.001358 ± 0.000079	126 ± 14	147.0 ± 8.5	1869.5 ± 8.8	9.5 ± 1.8
32.95	0.3996	236.53 ± 0.21	22.0 ± 1.8	4.6 ± 1.2	0.001477 ± 0.000036	262 ± 23	160.7 ± 3.9	1853.2 ± 4.1	4.6 ± 1.2
35.65	0.21855	101.31 ± 0.11	11.1 ± 3.2	6.2 ± 1.5	0.001484 ± 0.000079	224 ± 65	161.2 ± 8.6	1853.3 ± 8.8	6.2 ± 1.5
35.65	0.23286	152.62 ± 0.19	29.4 ± 3.0	5.1 ± 1.8	0.001723 ± 0.000077	147 ± 16	187.3 ± 8.4	1829.4 ± 8.8	5.1 ± 1.8
41.00	0.23140	365.05 ± 0.40	19.6 ± 3.0	6.4 ± 1.6	0.001705 ± 0.000055	523 ± 82	185.2 ± 6.0	1828.1 ± 6.0	6.4 ± 1.6
46.60	0.20286	216.07 ± 0.26	50.1 ± 3.4	9.0 ± 1.8	0.001452 ± 0.000059	103.3 ± 8.2	157.3 ± 6.4	1770.1 ± 7.1	9.0 ± 1.8
46.60	0.27950	182.66 ± 0.22	11.3 ± 2.5	10.8 ± 1.9	0.00225 ± 0.00012	602 ± 137	243 ± 13	1861 ± 13	10.8 ± 1.9
47.60	0.20568	146.86 ± 0.12	40.2 ± 3.4	8.2 ± 1.4	0.001968 ± 0.000083	119 ± 11	213.3 ± 9.0	1805.8 ± 9.7	8.3 ± 1.4
50.10	0.3801	240.37 ± 0.31	9.9 ± 1.8	4.8 ± 1.7	0.002141 ± 0.000089	861 ± 164	232.9 ± 9.7	1779.6 ± 9.7	4.8 ± 1.7
52.75	0.19978	161.95 ± 0.19	13.2 ± 3.5	6.6 ± 1.7	0.002423 ± 0.000077	492 ± 131	263.1 ± 8.4	1744.4 ± 8.5	6.6 ± 1.7
52.75	0.3447	223.14 ± 0.32	22.9 ± 2.0	5.6 ± 1.8	0.002481 ± 0.000059	399 ± 36	269.7 ± 6.4	1750.6 ± 6.6	5.6 ± 1.8
55.70	0.18103	172.38 ± 0.18	35.4 ± 3.8	7.4 ± 1.8	0.002351 ± 0.000095	189 ± 22	255 ± 10	1762 ± 11	7.4 ± 1.8
56.80	0.2442	245.80 ± 0.55	30.8 ± 2.9	3.2 ± 2.9	0.002417 ± 0.000057	318 ± 30	263.4 ± 6.2	1751.3 ± 6.4	3.2 ± 2.9
57.55	0.23711	142.07 ± 0.13	26.6 ± 2.9	6.5 ± 1.3	0.002501 ± 0.000071	221 ± 25	271.7 ± 7.8	1744.9 ± 8.2	6.5 ± 1.3
58.75	0.21828	156.06 ± 0.16	23.3 ± 3.2	6.7 ± 1.5	0.002385 ± 0.000071	264 ± 37	259.1 ± 7.8	1756.5 ± 8.0	6.7 ± 1.5
68.25	0.21947	124.52 ± 0.16	26.3 ± 3.2	7.2 ± 2.0	0.00250 ± 0.00026	196 ± 31	272 ± 28	1746 ± 29	7.2 ± 2.0
70.15	0.2322	148.03 ± 0.20	21.1 ± 3.0	6.8 ± 1.9	0.00272 ± 0.00008	316 ± 46	295.8 ± 9.0	1719.4 ± 9.2	6.8 ± 1.9
71.90	0.30160	227.11 ± 0.24	7.7 ± 2.3	7.8 ± 1.8	0.002781 ± 0.000078	1347 ± 403	301.8 ± 8.5	1711.0 ± 8.5	7.8 ± 1.8
73.65	0.3151	128.17 ± 0.22	16.0 ± 2.2	6.0 ± 2.3	0.003036 ± 0.000094	403 ± 57	330 ± 10	1685 ± 10	6.0 ± 2.3
78.25	0.15010	243.57 ± 0.31	22.3 ± 4.6	8.5 ± 2.2	0.003204 ± 0.000089	577 ± 121	347.5 ± 9.7	1714.8 ± 9.8	8.5 ± 2.2
91.65	0.21409	115.82 ± 0.15	32.8 ± 3.3	7.8 ± 2.1	0.00395 ± 0.00016	230 ± 25	429 ± 18	1667 ± 18	7.8 ± 2.1
93.30	0.21070	176.42 ± 0.23	38.6 ± 3.3	5.9 ± 1.7	0.004779 ± 0.000094	361 ± 32	520 ± 10	1692.7 ± 11	5.9 ± 1.7
100.5	0.21616	122.5 ± 0.12	33.4 ± 3.2	7.9 ± 1.7	0.00465 ± 0.00021	281 ± 30	505 ± 23	1591 ± 24	8.0 ± 1.7
105.70	0.1656	140.70 ± 0.18	17.3 ± 4.2	7.5 ± 1.9	0.00530 ± 0.00020	710 ± 174	576 ± 22	1498 ± 22	7.5 ± 1.9
75.88	0.85206	121.08 ± 0.11	11.15 ± 0.82	4.2 ± 1.4	0.002757 ± 0.000037	494 ± 37	300.2 ± 4.1	1543.1 ± 4.3	4.3 ± 1.4
81.23	1.00879	126.18 ± 0.11	6.85 ± 0.69	3.7 ± 1.4	0.002950 ± 0.000028	897 ± 91	321.4 ± 3.1	1514.4 ± 3.2	3.7 ± 1.4
94.03	0.6034	143.33 ± 0.13	8.9 ± 1.2	4.2 ± 1.4	0.004323 ± 0.000075	1143 ± 149	471.1 ± 8.3	1506.9 ± 8.3	4.2 ± 1.4
101.23	0.40424	140.12 ± 0.14	15.4 ± 1.7	4.5 ± 1.6	0.004516 ± 0.000051	680 ± 77	492.1 ± 5.7	1523.5 ± 5.9	4.5 ± 1.6
100.68	0.6377	136.11 ± 0.21	10.7 ± 1.1	2.7 ± 1.9	0.004652 ± 0.000066	979 ± 101	507.8 ± 6.2	1537.6 ± 6.3	2.7 ± 1.9
101.23	0.66251	144.06 ± 0.24	8.2 ± 1.1	2.2 ± 2.3	0.004364 ± 0.000046	1271 ± 164	476.6 ± 5.2	1438.8 ± 5.2	2.2 ± 2.3
106.98	0.52911	112.38 ± 0.13	23.5 ± 1.3	4.3 ± 1.8	0.005865 ± 0.000058	463 ± 26	639.6 ± 6.4	1378.5 ± 7.0	4.3 ± 1.8

05FC-04 Depth (cm)	Weight g	^{238}U ppb	^{232}Th ppt	δ^{234}U measured[a]	$[^{230}$Th/^{238}U] activity[c]	$[^{230}$Th/^{232}Th] ppm[d]	Age uncorrected	Year CE[c,e]	δ^{234}U$_{initial}$ corrected[b]
0.020	0.20850	354.39 ± 0.39	14.0 ± 3.3	5.3 ± 1.1	0.000345 ± 0.000039	145 ± 38	37.5 ± 4.2	1975.5 ± 4.2	5.3 ± 1.1
4.665	0.38044	232.36 ± 0.29	19.6 ± 1.8	4.8 ± 1.9	0.000732 ± 0.000043	144 ± 16	79.6 ± 4.6	1934.6 ± 4.8	4.8 ± 1.9
12.765	0.36680	226.79 ± 0.19	16.7 ± 1.9	4.4 ± 1.2	0.001142 ± 0.000044	256 ± 31	124.2 ± 4.8	1889.7 ± 4.9	4.4 ± 1.2
16.755	0.33310	217.71 ± 0.21	9.9 ± 2.1	7.1 ± 1.5	0.001224 ± 0.000094	443 ± 99	133 ± 10	1880 ± 10	7.1 ± 1.5

Analytical errors are 2σ of the mean.

[a] δ^{234}U = $([^{234}$U/^{238}U]$_{activity} - 1) \times 1000$.

[b] δ^{234}U$_{initial}$ corrected was calculated based on ^{230}Th age (T), i.e., δ^{234}U$_{initial} = \delta^{234}U_{measured} X e^{\lambda 234 \cdot T}$, and T is corrected age.

[c] $[^{230}$Th/^{238}U]$_{activity} = 1 - e^{-\lambda_{230}T} + (\delta^{234}U_{measured}/1000)[\lambda_{230}/(\lambda_{230} - \lambda_{234})](1 - e^{-(\lambda_{230}-\lambda_{234})T})$, where T is the age. Decay constants are 9.1577×10^{-6} yr^{-1} for ^{230}Th, 2.8263×10^{-6} yr^{-1} for ^{234}U, and 1.55125×10^{-10} yr^{-1} for ^{238}U (Cheng et al., 2000; Jaffey et al., 1971).

[d] The degree of detrital ^{230}Th contamination is indicated by the $[^{230}$Th/^{232}Th] atomic ratio instead of the activity ratio.

[e] Age corrections were calculated using an estimated atomic ^{230}Th/^{232}Th ratio of 4 ± 2 ppm.

Title Page

Abstract | Introduction

Conclusions | References

Tables | Figures

|◄ | ►|

◄ | ►

Back | Close

Full Screen / Esc

Printer-friendly Version

Interactive Discussion

Table 2. Summary of dripwater, predicted and actual calcite δ^{18}O values.

	Mean Annual Temperature: Forestry Cave Drip	26.5 °C Jacob's Cave Drip 1	Jacob's Cave Drip 2	2σ uncertainty
Measured δ^{18}O (‰ VSMOW)	−6.79	−6.85	−6.60	±0.20
Kim and O'Neil Calcite (lab) δ^{18}O (‰ VPDB)	−9.17	−9.23	−8.98	±0.20
Tremaine Calcite (cave) δ^{18}O (‰ VPDB)	−8.05	−8.11	−7.86	±0.20
			10FC-02 Tip δ^{18}O (‰ VPDB)	2σ uncertainty
			−7.59	±0.12

Fig. 1. Regional rainfall patterns in the tropical Indo-Pacific tropics based on data from Kummerow et al. (2000). White triangle in all panels denotes the study site. Rectangles in each panel qualitatively highlight the broader tropical SPCZ domain. **(a)** Annual mean surface precipitation in the tropical Indo-Pacific from 1998–2011. **(b)** Spatial correlation (r) between monthly rainfall anomalies at the study site and rainfall anomalies in the southwestern Pacific. Anomalies are relative to the 1998–2011 climatology. **(c)** Map of significance (p values) for panel **(b)**. Note both the regional significance of rainfall variability at the study site, as well as the prominent correlation dipole in panel **(b)** and **(c)** south of the equator, spanning from 150° E to 120° W, indicative of northeast-southwestward SPCZ movement.

Full Screen / Esc

Printer-friendly Version

Interactive Discussion

Fig. 2. Cross-sectional image of the Guadalcanal stalagmite (10FC-02), which is ∼ 1.1 m in length. Samples for stable isotope analyses were extracted along paths shown by black lines at 500 µm increments. Note that not all paths are on the same sides of the slabs as depicted. This is to maintain sampling transects on an ideal axis of maximum growth and the center of the growth axis.
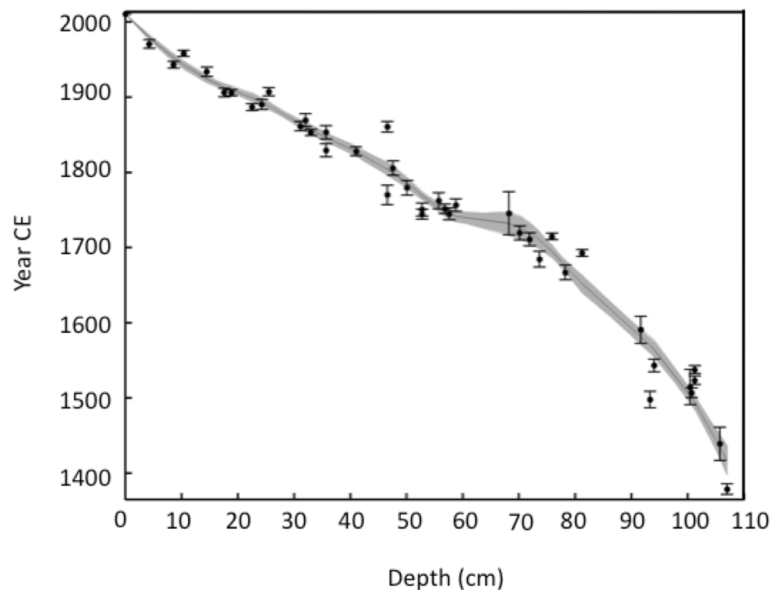
Fig. 3. Growth history of 10FC-02 stalagmite. Black symbols indicate individual U-Th ages with error bars corresponding to ±2σ uncertainty. A Monte Carlo method of fitting cubic splines to the ages and respective ±2σ age uncertainties is illustrated by the median age model (thin black line), which assumes no analytical error, and gray cloud which represents all 10 000 alternative age models generated.
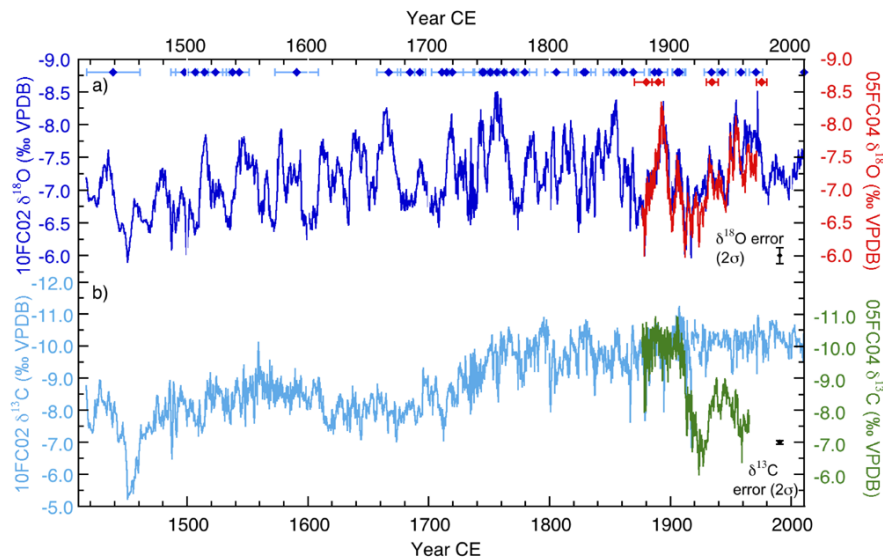
Fig. 4. Time series of paired **(a)** δ^{18}O and **(b)** δ^{13}C in 10FC-02 and 05FC-04 stalagmites. Blue diamonds with horizontal error bars illustrate the locations of 10FC-02 U-Th ages and their respective ±2σ errors. The vertical error bars denote respective ±2σ uncertainties for isotopic measurements. Note the strong reproducibility in the δ^{18}O mean and variability in the two stalagmites, and the lack of reproducibility in the δ^{13}C records. The correlation coefficient between the 10FC-02 oxygen and carbon isotope time series is 0.11. The average absolute difference in time between original and adjusted timescales on the 05FC-04 stalagmite is 4.95 yr, whereas the average uncertainty for the 05FC-02 stalagmite U-Th dates is ±6.0 yr.
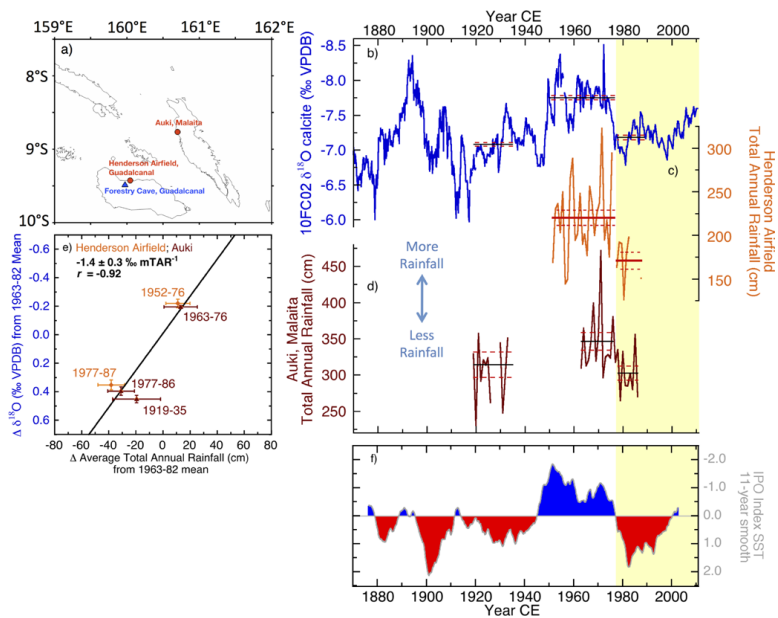
Full Screen / Esc

Printer-friendly Version

Interactive Discussion

Fig. 5. Stalagmite δ^{18}O variations compared with rain gauge data. **(a)** Location of rain gauges (red circles) and Forestry Cave (blue triangle) in the Solomon Islands. **(b)** Modern portion of the 10FC-02 stalagmite δ^{18}O record. Total annual rainfall at **(c)** Henderson Airfield, Honiara, Guadalcanal, and **(d)** Auki, Malaita, Solomon Islands (Deser et al., 2004; Vose et al., 1992). Horizontal lines in represent pre- and post-1976 means plotted with standard errors. Post-1976/1977 regime shift is shaded beige. **(e)** Relationship between changes in stalagmite δ^{18}O and changes in total annual rainfall amount in rain gauge data. Means and standard errors were calculated for rain gauge and stalagmite δ^{18}O records during contemporaneous intervals in which data exists for both time series, with pre- and post-1976/1977 regime shift separated into two discrete intervals (the Auki time series allows for an additional comparison interval from the early twentieth century). Labels indicate the interval over which means were calculated. Means for each of the three respective time series over the only time interval in which all three overlap, 1963–1982, were removed from respective values in order to standardize the cross plot to account for the difference in total rainfall amount at Auki and Henderson Airfield. Panel **(f)** illustrates the larger scale nature of 1976/1977 regime shift through the global SST-derived Interdecadal Pacific Oscillation (IPO) index (Folland et al., 2002).
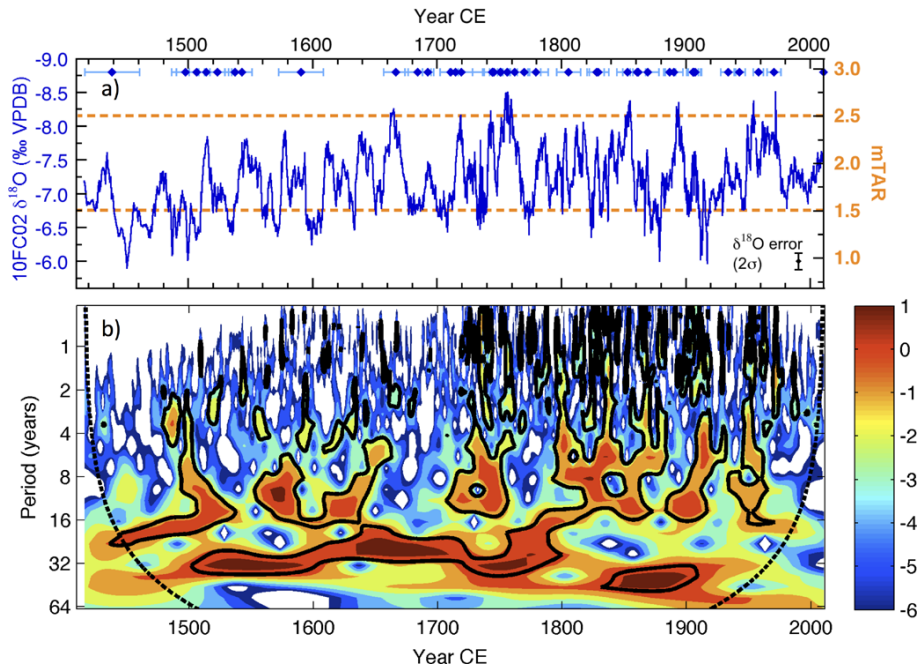
Fig. 6. (a) Stalagmite $\delta^{18}O$ record, plotted as isotopic variation (left axis) and as variations in total annual rainfall amount in meters (mTAR; right axis). Symbols and error bars as in Fig. 5. Horizontal dashed lines frame the time series for context about two mTAR with a one mTAR range. **(b)** Rectified wavelet power (in base 2 logarithm of standard deviation units) spectrum of stalagmite time series (Liu et al., 2007; Torrence and Compo, 1998). Black contours denote power above the 95 % confidence interval when using an AR(1) red noise model, dotted lines denote "cone of influence" from padding with zeros (see Torrence and Compo, 1998). The $\pm 2\sigma$ analytical uncertainty range in $\delta^{18}O$ (± 0.20 ‰) corresponds to $-3.5\log_2$ std. dev. units in wavelet spectrum power.
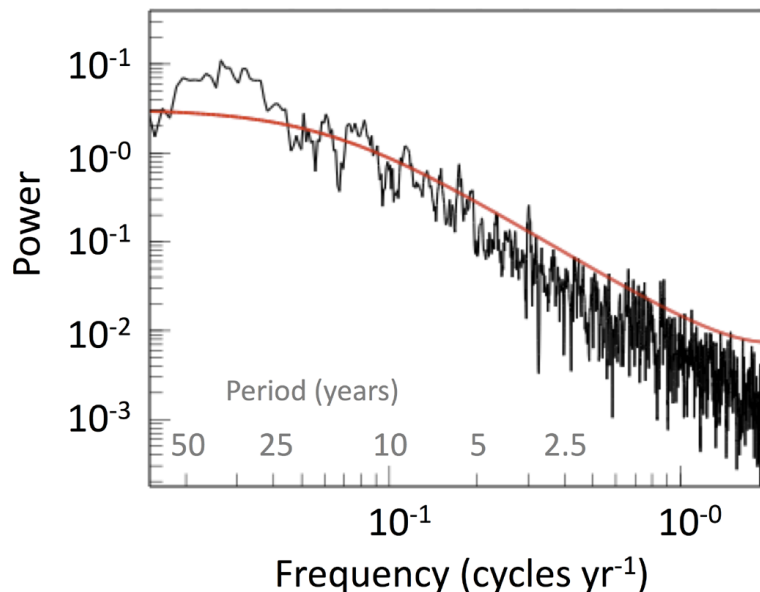
Fig. 7. Multi-Taper Method (MTM) spectrum of the median stalagmite δ^{18}O time series. The red line denotes the 99 % confidence intervals, respectively, for an AR(1) red noise model calculated from the 10FC-02 stalagmite time series. The MTM analysis was performed using the K-Spectra software package (http://www.spectraworks.com/). Note significant concentrations of power throughout the interannual and multidecadal bandwidth.
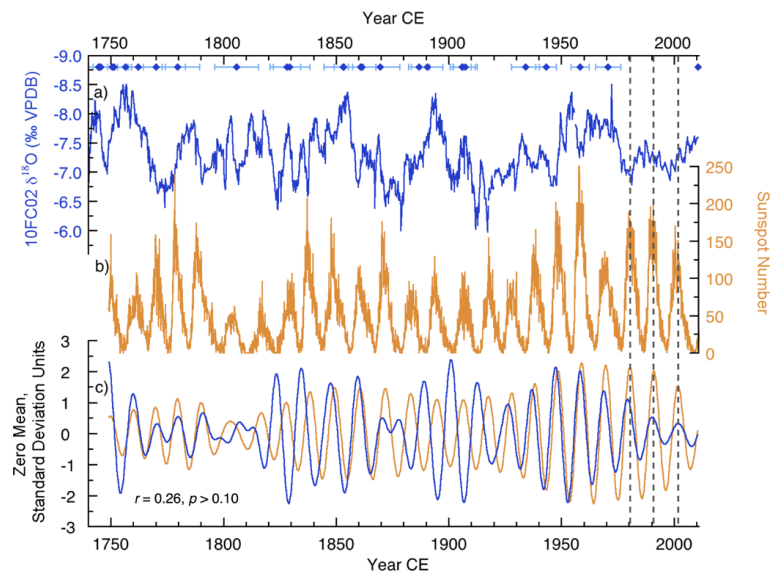
Fig. 8. Comparison between stalagmite δ^{18}O variations **(a)** and a record of the sunspot cycle from 1749–2009 that has a strong 11 yr period **(b)**. Panel **(c)** shows both records filtered using a Gaussian window with a central frequency of 0.091 ± 0.02 (bandwidth) cycles yr^{-1} (or ~ 11 yr) and standardized to zero mean unit variance. The correlation between the two is only significant at the 90 % confidence interval when the effective degrees of freedom (edf) are adjusted for serial autocorrelation (edf = 48). The sunspot record contains 24 clear cycles. The stalagmite record contains 25 cycles based on the number of independent data points in the filtered record ($dy/dt = 0$). Note that there is no systematic relationship in phasing or amplitude modulation that would lead us to consider a causative forcing from sunspot counts. The average uncertainty for the stalagmite age model is ± 1.5 yr (2σ) over the interval of comparison. The most recent three peaks of sunspot activity used by (Matthews, 2011; Meehl et al., 2009) to hypothesize a response in SPCZ precipitation are marked by vertical dashed lines.
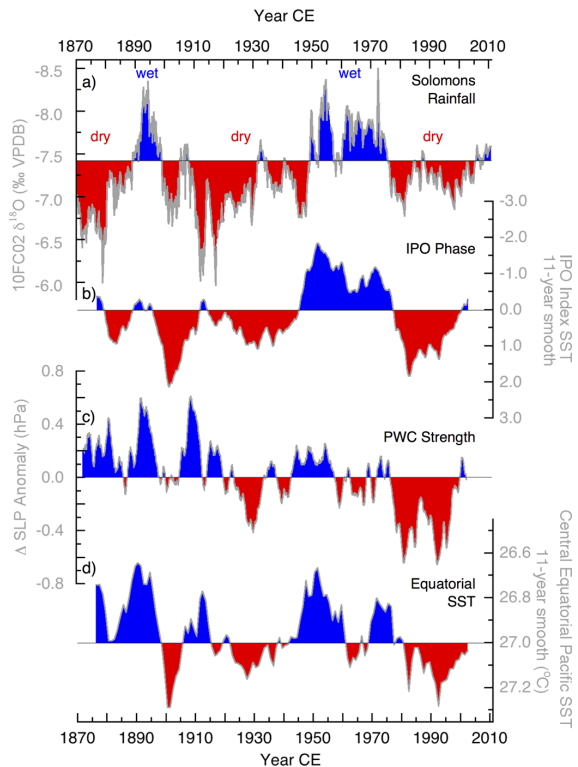
Fig. 9. Comparison of timing in phase changes in stalagmite δ^{18}O **(a)** with identified state changes in ocean and atmospheric variables since 1870. **(b)** Interdecadal Pacific Oscillation Index (IPO) of SST anomalies (Folland et al., 2002). **(c)** Sea level pressure (SLP) gradient anomaly as calculated by Vecchi et al. (2006), taken in literature as a surface expression of Pacific Walker Circulation (PWC) strength. **(d)** 11 yr running average of annual mean central tropical Pacific SST over 5° S to 5° N, 120° W to 170° W, illustrating a relative warm or cool central Pacific SST during each phase. Identified phases occurred from 1925 through 1946 (22 yr), 1947 through 1976 (30 yr), and 1977 through 1995 (19 yr).

Title Page

Abstract | Introduction

Conclusions | References

Tables | Figures

|◄ | ►|

◄ | ►

Back | Close

Full Screen / Esc

Printer-friendly Version

Interactive Discussion